# Spatial-Wideband Effect in Line-of-Sight MIMO Communication

Mohammad M. Mojahedian
*Member, IEEE*
Univ. Pompeu Fabra, Barcelona
mohammadmahdi.mojahedian@upf.edu

Masoud Attarifar
*Member, IEEE*
Univ. Pompeu Fabra, Barcelona
masoud.attarifar@upf.edu

Angel Lozano
*Fellow, IEEE*
Univ. Pompeu Fabra, Barcelona
angel.lozano@upf.edu

*Abstract*—This paper addresses the spatial-wideband effect in line-of-sight multiple-input multiple-output channels. This effect arises once the bandwidth is large enough that the differences in propagation delays for distinct transmit-receive antenna pairs cease to be negligible relative to the symbol period; this, in turn, gives rise to intersymbol interference. The impact of this effect is quantified as a function of the relevant geometric parameters (range, array orientations, antenna spacings) and a family of scalable solutions is proposed to counter it. In particular, a solution based on per-antenna delay lines at transmitter and receiver is shown to be highly effective, and a criterion is derived to set those delay lines as a function of the channel.

*Index Terms*—Line-of-sight communication, multiple-input multiple-output, spatial-wideband effect, beam squint, precoding.

## I. Introduction

In search of ever wider bandwidths, wireless systems continue to move to progressively higher frequencies. With 5G currently seizing mmWave bands, the attention of researchers is shifting to the subterahertz range (0.1–1 THz) [1]. Recent experimental demonstrations with state-of-the-art solid-state electronics have reached 100 Gb/s over 20 GHz of bandwidth at 300 GHz [2].

By virtue of the minute wavelength, the subterahertz realm offers additional opportunities besides lots of idle spectrum: multiple-input multiple-output (MIMO) transmission becomes feasible in line-of-sight (LOS) conditions [3]–[14]. Precisely, a high-rank channel matrix can be obtained in the absence of multipath propagation, based only on the array apertures themselves, as the receive array becomes—in wavelengths—large enough to resolve each transmit antenna. This is a welcome phenomenon given that LOS is the predominant propagation mechanism for the envisioned short-range transmissions at these very high frequencies.

In multipath channels, wide bandwidths inevitably lead to frequency selectivity and intersymbol interference (ISI) because of the distinct delays over the multipath components. As illustrated with a two-path toy setting in Fig. 1, these delay differences arise chiefly because of the distinct lengths of the propagation paths; additional differences exist across antennas, given their slightly displaced positions, but these are comparatively negligible. In LOS channels, only the direct propagation path is present and hence there are no multipath-induced delays, but the antenna-specific differences remain
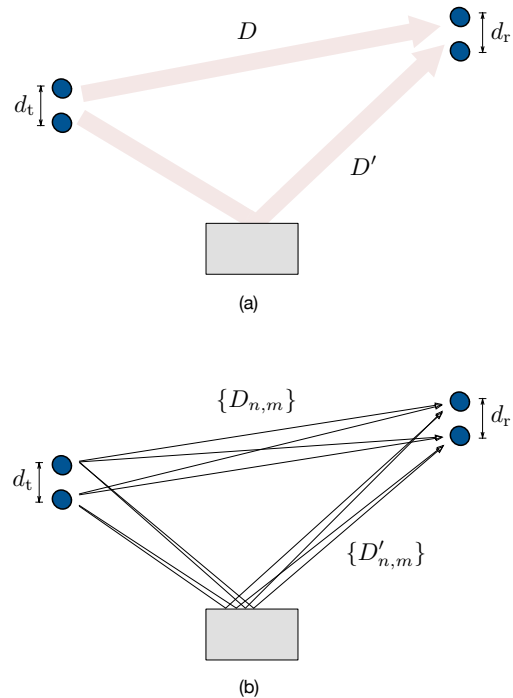


Fig. 1. Two-path channel. (a) Path delay differences. (b) Antenna-specific delay differences.

and the enormous bandwidths amplify their role. Once these become nonnegligile relative to the symbol period, frequency selectivity and ISI arise. To refer to this specific kind of frequency selectivity, the term *spatial-wideband* has been coined [15].

When transmitter and receiver implement phased-array beamforming in LOS, the spatial-wideband effect manifests itself as a drift in the beam directions over frequency, a phenomenon known as *beam squint* [16]–[18]. This phenomenon can be prevented by implementing true time delay beamforming, whereby, rather than antenna-specific phase shifts, antenna-specific delays are applied [19]–[21]. An example of true time delay transmit beamforming is provided in Fig. 2.

In LOS MIMO with spatial multiplexing, the correction of the spatial-wideband effect becomes far less straightforward: from the vantage of each receive antenna, a different set of
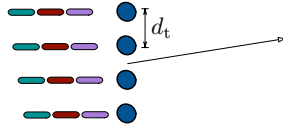
Fig. 2. True time delay transmit beamforming, with the sequence of symbols radiated by each antenna shown explicitly. The delay across the array determines the beamforming direction.

delays should generally be applied to each transmit antenna, and vice versa. This problem motivates the present paper, whose contributions are:

- A quantification of the impact of the spatial-wideband effect in wideband LOS MIMO channels.
- The derivation of a family of scalable transmitter and receiver solutions to counter this effect.

The focus is on uniform linear arrays (ULAs), which experience the most severe spatial-wideband effects for a given number of antennas, yet the proposed solutions apply to arbitrary array topologies.

## II. CHANNEL MODEL

Consider an LOS setting with respective ULAs featuring $N_\text{t}$ transmit and $N_\text{r}$ receive antennas. As illustrated in Fig. 3, the ULA orientations can be specified through the corresponding elevation angles, $\theta_\text{t}$ and $\theta_\text{r}$, plus one azimuth angle, $\phi$.

### A. Narrowband Representation

Let us begin by considering a narrowband situation, with negligible differences in the delays over the links connecting the various transmit and receive antennas. Then, the channel between the $m$th transmit and the $n$th receive antenna adopts the form of the complex coefficient

$$\frac{\sqrt{G_\text{t} G_\text{r}}\,\lambda}{4\pi D_{n,m}}\, e^{-j\frac{2\pi}{\lambda} D_{n,m}} \qquad \begin{aligned} n &= 0,\ldots,N_\text{r}-1 \\ m &= 0,\ldots,N_\text{t}-1 \end{aligned} \qquad (1)$$

where $D_{n,m} = \sqrt{D_x^2 + D_y^2 + D_z^2}$ is the distance, given

$$D_x = n d_\text{r} \cos\theta_\text{r} - m d_\text{t} \cos\theta_\text{t}, \qquad (2)$$
$$D_y = n d_\text{r} \sin\theta_\text{r} \sin\phi, \qquad (3)$$
$$D_z = D + n d_\text{r} \sin\theta_\text{r} \cos\phi - m d_\text{t} \sin\theta_\text{t}, \qquad (4)$$

whereas $\lambda$ is the wavelength and $G_\text{t}$, $G_\text{r}$, are the antenna gains in the appropriate direction.

Provided the array apertures are small relative to $D_{n,m}$, the magnitude of (1) can be regarded as constant across $n$ and $m$ and the channel matrix can be normalized into

$$\boldsymbol{H} = \begin{bmatrix} e^{-j\frac{2\pi}{\lambda} D_{0,0}} & \ldots & e^{-j\frac{2\pi}{\lambda} D_{0,N_\text{t}-1}} \\ \vdots & \ddots & \vdots \\ e^{-j\frac{2\pi}{\lambda} D_{N_\text{r}-1,0}} & \ldots & e^{-j\frac{2\pi}{\lambda} D_{N_\text{r}-1,N_\text{t}-1}} \end{bmatrix}. \qquad (5)$$

The receiver observes

$$\boldsymbol{y} = \boldsymbol{H}\boldsymbol{x} + \boldsymbol{z}, \qquad (6)$$
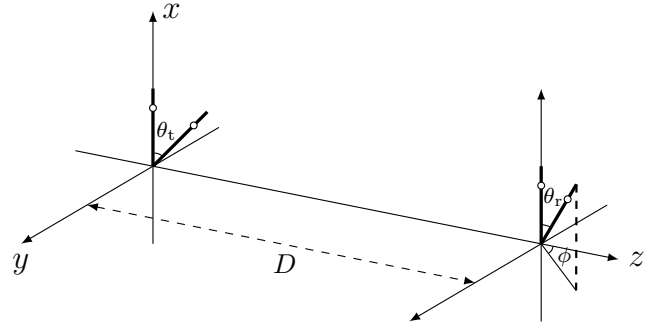


Fig. 3. LOS MIMO setting with transmit and receive ULAs.

where $\boldsymbol{z} \sim \mathcal{N}_\mathbb{C}(\boldsymbol{0}, N_0 B \boldsymbol{I})$ and $\boldsymbol{x} = \sqrt{P}\boldsymbol{F}\boldsymbol{s}$ is the transmit signal, with $\boldsymbol{s}$ a vector of unit-power symbols and $\boldsymbol{F}$ the precoder satisfying $\text{tr}(\boldsymbol{F}\boldsymbol{F}^*) = 1$ such that $P$ is the radiated power. In turn, $N_0$ is the noise spectral density and $B$ is the bandwidth.

By precoding along the right singular vectors of $\boldsymbol{H}$, with powers optimized via waterfilling, while receiving along the left singular vectors, capacity can be achieved [22]. This entails the singular-value decomposition (SVD) of $\boldsymbol{H}$.

### B. Spatial-Wideband Effect

As the bandwidth and/or the arrays grow large, the delay differences become nonnegligible relative to the symbol period, and they must be accounted for in the formulation. The $n$th receive antenna observes

$$y_n(t) = \sum_{m=0}^{N_\text{t}-1} x_m(t - \tau_{n,m})\, e^{-j\frac{2\pi}{\lambda} D_{n,m}} + z_n(t) \qquad (7)$$

with $\tau_{n,m} = D_{n,m}/c$ the delay experienced by the signal from the $m$th transmit antenna and

$$x_m(t) = \sqrt{P} \sum_{k=1}^{K} f_{m,k}\, s_k(t) \qquad (8)$$

where $f_{m,k}$ is the $(m,k)$th entry of $\boldsymbol{F}$ and

$$s_k(t) = \sum_{i=-\infty}^{\infty} s_{k,i}\, g(t - i/B) \qquad (9)$$

is the $k$th data stream, for $k = 1,\ldots,K$, with $\{s_{k,i}\}$ being unit-power symbols and $g(\cdot)$ a unit-energy pulse. (The symbol period has been taken to be $1/B$, with a corrective factor being necessary if the pulse shape consumes excess bandwidth.)

For given $\theta_\text{t}$ and $\theta_\text{r}$, increasing $\phi$ is sure to reduce the delays, hence we can conservatively concentrate on $\phi = 0$. And, as in conventional ISI channels, a key figure of merit is the *delay spread*

$$\sigma_\tau = \sqrt{\frac{1}{N_\text{t} N_\text{r}} \sum_m \sum_n \tau_{n,m}^2 - \left(\frac{1}{N_\text{t} N_\text{r}} \sum_m \sum_n \tau_{n,m}\right)^2}, \qquad (10)$$

whose definition is simpler than in conventional ISI channels by virtue of the power being the same for all the terms.
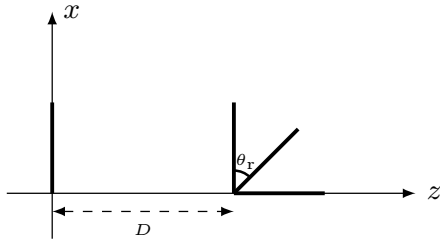
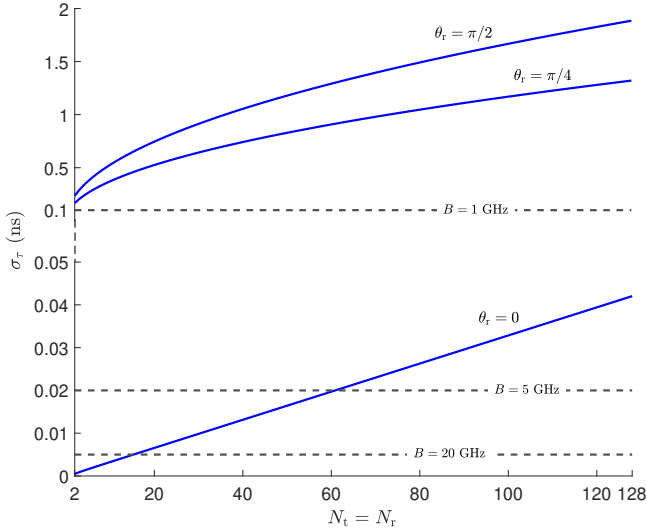Fig. 4. Vertical transmit array with a receive array at elevation $\theta_r$.



Fig. 5. Delay spread as a function of $N_t = N_r = N$ at 300 GHz, with $D = 30$ m and $d_t = d_r = \sqrt{\lambda D / N}$. The threshold $0.1/B$ is indicated for $B = 1$, 5, and 20 GHz.

Once the condition $\sigma_\tau B \ll 1$ is violated, the narrowband representation set forth in Sec. II-A no longer suffices and a transmit-receive architecture oblivious to this may experience a severe performance degradation. Based on the rule of thumb from ISI channels that the degradation becomes considerable for $\sigma_\tau B \gtrsim 0.1$, we can delineate the regimes where the spatial-wideband effect might arise. For a representative assessment, consider the situation in Fig. 4, where the transmitter is vertical and the receiver is oriented as per $\theta_r$. The corresponding delay spreads in Fig. 5 evince that, for $\theta_r \geq 45°$ and $B \geq 1$ GHz, the effect might arise even for two-antenna arrays; with substantially more than two antennas, it might arise for bandwidths of only a few hundred MHz. The robustness increases somewhat as $\theta_r$ approaches zero, but, even then, the effect might arise for multi-GHz bandwidths. As illustrated in Sec. IV, the effect indeed arises in all of these situations and the ensuing performance degradation is dire.

## III. INFORMATION-THEORETIC CAPACITY

The channel is regarded as static, hence known by both transmitter and receiver. In the frequency domain, and with the observations at the $N_r$ receive antennas assembled into a vector, (7) becomes

$$\mathbf{y}(f) = \mathbf{H}(f)\,\mathbf{x}(f) + \mathbf{z}(f) \qquad -\frac{B}{2} \leq f \leq \frac{B}{2} \qquad (11)$$

where

$$\mathsf{h}_{n,m}(f) = e^{-j\frac{2\pi}{\lambda} D_{n,m}}\, e^{-j2\pi f \tau_{n,m}} \qquad (12)$$

whose second term reflects the frequency-selective nature of the channel on account of the spatial-wideband effect. If the Fourier transform of the pulse shape, $G(f) = \mathcal{F}\{g(\tau)\}$, is not flat over the signal bandwidth, it can be absorbed into $\mathsf{h}_{n,m}(f)$.

Applying, now as a function of frequency, the SVD-based strategy sketched in Sec. II-A, the capacity emerges as

$$C = \frac{1}{B} \sum_{k=0}^{N_{\min}-1} \int_{-B/2}^{B/2} \log_2\left(1 + \frac{P}{N_0}\left[\frac{1}{\gamma} - \frac{1}{\sigma_k^2(f)}\right]^+ \sigma_k^2(f)\right) df \qquad (13)$$

with $\sigma_k(f)$ the $k$th singular value of $\mathbf{H}(f)$ while $\gamma$ satisfies

$$\sum_{k=0}^{N_{\min}-1} \int_{-B/2}^{B/2} \left[\frac{1}{\gamma} - \frac{1}{\sigma_k^2(f)}\right]^+ df = 1 \qquad (14)$$

given $[z]^+ = \max(0, z)$.

Approaching (13) via optimum transmission and reception in the frequency domain involves a progressively finer partition into subbands with a correspondingly growing number of SVDs. This motivates the interest in alternative solutions that are scalable, which is the subject of the next section.

## IV. SCALABLE WIDEBAND MIMO

### A. Frequency-Domain Approach

A scalable approach inspired directly on the formulation of the capacity would be to partition the available bandwidth into $L$ subbands, with $L$ being a tradeoff between performance and complexity. (For $L = 1$ we recover the scheme based on the narrowband representation whereas, for $L \to \infty$, we obtain the capacity-achieving solution.) This approach, entertained already for beamforming [23], can be applied to general MIMO settings by replacing the per-subband beamforming with per-subband SVD-based transmission and reception.

Letting $\mathbf{H}_\ell$ be the channel at the center frequency of the $\ell$th subband, with SVD given by $\mathbf{H}_\ell = \mathbf{U}_\ell \mathbf{\Sigma}_\ell \mathbf{V}_\ell^*$ where $\mathbf{\Sigma}_\ell = \text{diag}\big(\sigma_{\ell,0}, \ldots, \sigma_{\ell,N_{\min}-1}\big)$, the transmit-receive relationship over that subband is [24, sec. 5.3]

$$\mathbf{U}_\ell^* \mathbf{y}_\ell(f) = \sqrt{P}\, \mathbf{U}_\ell^* \mathbf{H}(f) \mathbf{V}_\ell \, \text{diag}\big(\sqrt{p_{\ell,0}}, \ldots, \sqrt{p_{\ell,N_{\min}-1}}\big)\, \mathbf{s}_\ell$$
$$+ \mathbf{U}_\ell^* \mathbf{z}_\ell(f) \qquad (15)$$

where $p_{\ell,k}$ is the power allocated to the $k$th data stream on the $\ell$th subband and $\mathbf{U}_\ell^* \mathbf{z}_\ell(f) \sim \mathbf{z}_\ell(f)$. The signal-to-interference-plus-noise ratio (SINR) experienced by the $k$th stream over the $\ell$th subband is then

$$\text{sinr}_{\ell,k}(f) = \frac{p_{\ell,k}\,|\mathbf{u}_{\ell,k}^* \mathbf{H}(f)\mathbf{v}_{\ell,k}|^2}{\sum_{k' \neq k} p_{\ell,k'}\,|\mathbf{u}_{\ell,k}^* \mathbf{H}(f)\mathbf{v}_{\ell,k'}|^2 + \frac{1}{L}\frac{N_0 B}{P}} \qquad (16)$$
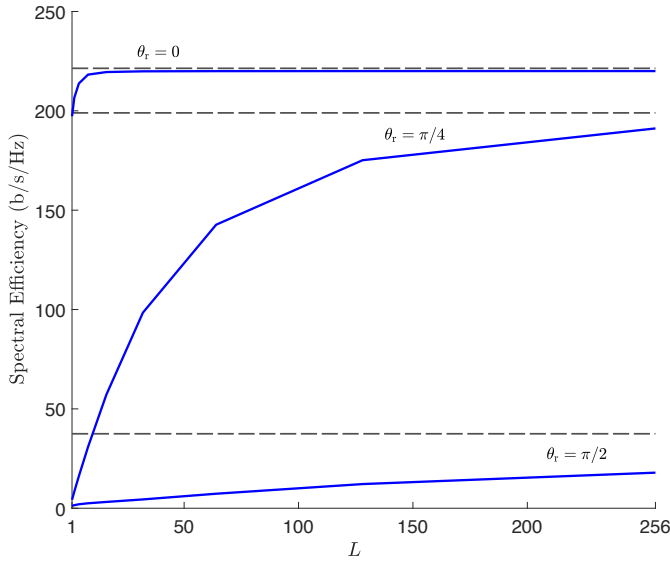
Fig. 6. Spectral efficiency versus $L$ with $N_t = N_r = 64$, $D = 30$ m, $\frac{P}{N_0 B} = 10$ dB, $f_c = 300$ GHz, and $B = 20$ GHz. In dashed, the corresponding narrowband capacity.

where

$$p_{\ell,k} = \left[ \frac{1}{\gamma} - \frac{1}{\sigma_{\ell,k}^2} \right]^+ \qquad (17)$$

with $\gamma$ such that $\sum_k \sum_\ell p_{\ell,k} = 1$. The achievable spectral efficiency is

$$C = \frac{1}{B} \sum_{k=0}^{N_{\min}-1} \sum_{\ell=1}^{L} \int_{-\frac{B}{2}+\frac{(\ell-1)B}{L}}^{-\frac{B}{2}+\frac{\ell B}{L}} \log_2\Big(1 + \mathsf{sinr}_{\ell,k}(f)\Big)\, df. \qquad (18)$$

This spectral efficiency is exemplified in Fig. 6, which evidences how, for some receiver orientations, very few subbands suffice to converge to the capacity whereas, for other orientations, the convergence is excruciatingly slow and the scalability is called into question.

### B. Delay-Domain Approach

While the division into a few subbands is an obvious way of counterbalancing the increase in bandwidth, it is only effective for a restricted set of orientations. A delay-domain approach generalizing the principles of true time delay beamforming is therefore enticing.

Given per-antenna delay lines as in Fig. 7, the challenge is to set those delays, denoted by $\alpha_1, \ldots, \alpha_{N_t}$ at the transmitter and by $\beta_1, \ldots, \beta_{N_r}$ at the receiver. However, as advanced in Sec. I, the optimum corrective delay for a certain transmit antenna is in general different from the viewpoint of each receive antenna, and vice versa. Save for singular situations such as $\theta_t = \theta_r = 0$, it is not possible to simultaneously equalize the delays for the antenna pairs. In fact, the transmissions from the $N_t$ transmit antennas often do not even reach every receive antenna in the same order.
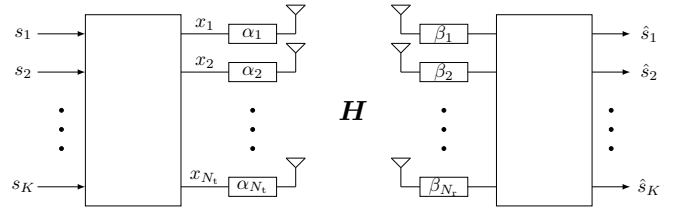


Fig. 7. MIMO setting with per-antenna delay lines at transmitter and receiver.

A strategy that is consistent with the delay spread being a key figure of merit is to minimize the *overall* delay spread, including transmitter, channel, and receiver. That means setting the transmit and receive delay lines to

$$(\alpha_m^*, \beta_n^*) = \arg\min_{\alpha_m, \beta_n} \frac{1}{N_t N_r} \sum_m \sum_n \left( \tau_{n,m} + \beta_n + \alpha_m \right)^2$$
$$- \left( \frac{1}{N_t N_r} \sum_m \sum_n \left( \tau_{n,m} + \beta_n + \alpha_m \right) \right)^2, \quad (19)$$

which is solved by

$$\beta_n^* = -\frac{1}{N_t} \sum_{m=0}^{N_t-1} \tau_{n,m} + \frac{\mu}{N_t N_r} \sum_{m=0}^{N_t-1} \sum_{n=0}^{N_r-1} \tau_{n,m} \qquad (20)$$

$$\alpha_m^* = -\frac{1}{N_r} \sum_{n=0}^{N_r-1} \tau_{n,m} + \frac{1-\mu}{N_t N_r} \sum_{m=0}^{N_t-1} \sum_{n=0}^{N_r-1} \tau_{n,m} \qquad (21)$$

where $\mu$ is an arbitrary value in $[0, 1]$.

Denoting by $\mathbf{H}^{\text{eff}}(f)$ the overall channel frequency response with the transmit and receive delay lines subsumed, such that

$$\mathsf{h}_{n,m}^{\text{eff}}(f) = e^{-j\frac{2\pi}{\lambda} D_{n,m}}\, e^{-j2\pi f(\tau_{n,m}+\alpha_m^*+\beta_n^*)}, \qquad (22)$$

the SINR and spectral efficiency are given by (16)–(18), with $\mathbf{H}_{\text{eff}}(f)$ in lieu of $\mathbf{H}(f)$ and with $L = 1$.

### C. Combined Approach

The frequency- and delay-domain approaches can be combined by partitioning the bandwidth into $L$ subbands and setting the delay lines to respective values obtained by solving (20) and (21) on each subband.

## V. PERFORMANCE EVALUATION

To evaluate the performance of solution propounded in the previous section, let us again consider the situation in Fig. 4, where the transmitter is vertical and the receiver is oriented as per $\theta_r$.

Shown in Fig. 8 is the spectral efficiency as a function of $\theta_r$. While the information-theoretic capacity of a 20-GHz channel is essentially identical to that of a narrowband channel, a solution oblivious to the spatial-wideband effect performs catastrophically in most orientations. With the introduction of delay lines at transmitter and receiver, a hefty share of the shortfall is recovered and, with a further partition into a few subbands, the recovery is almost complete. For $\theta_r = 0$, interestingly, the introduction of delay lines with the criterion
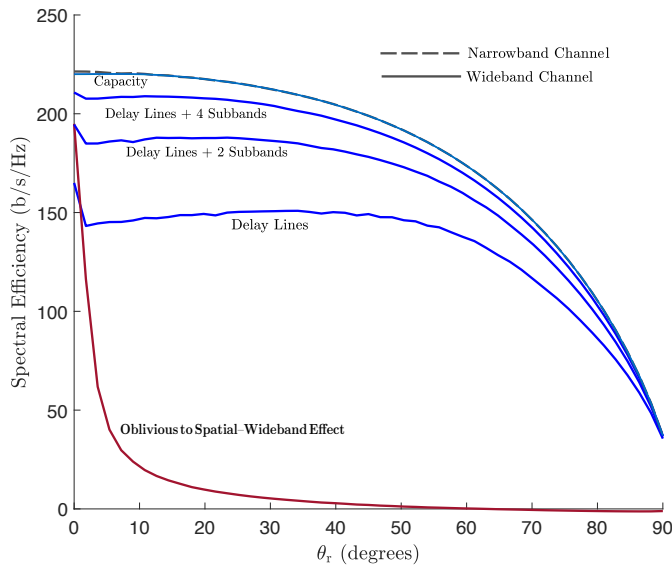
Fig. 8. Spectral efficiency versus $\theta_{\mathrm{r}}$ with $N_{\mathrm{t}} = N_{\mathrm{r}} = 64$, $D = 30$ m, $P/N_0 B = 10$ dB, and $f_{\mathrm{c}} = 300$ GHz. The dashed line indicates $B/f_{\mathrm{c}} \ll 1$ while the solid lines indicate $B = 20$ GHz (capacity and various solutions, including being oblivious to the spatial wideband effect).



Fig. 9. Spectral efficiency vs bandwidth for $N_{\mathrm{t}} = N_{\mathrm{r}} = 64$, $D = 30$ m, $P/N_0 B = 10$ dB at $B = 20$ GHz, and $f_{\mathrm{c}} = 300$ GHz. For each orientation, the top curve indicates the capacity whereas the bottom curve corresponds to delay lines with the criteria in (20)–(21).

in (20)–(21) is counterproductive, suggesting that even better criteria may be possible.

Concentrating on the pure delay-domain solution, Fig. 9 shows how its gap to optimality changes as the bandwidth is swept from $B = 1$ GHz to $B = 20$ GHz, for different orientations. In every case, the performance is excellent, and would improve further with any division into subbands. Finally, Fig. 10 confirms that the performance degradation in transmissions oblivious to the spatial-wideband effect begins, for some orientations, with bandwidths of a few hundred MHz. This reinforces the importance of solutions such as the ones presented herein. And, for $\theta_{\mathrm{r}} = 0$, the figure again suggests that even better criteria than (20)–(21) may exist.

## VI. SUMMARY

In LOS MIMO, the performance deteriorates rapidly as the bandwidth grows due to the spatial-wideband effect. For most array orientations, the degradation becomes noticeable for rather modest bandwidths, sometimes well below 1 GHz. The parallel arrangement of transmitter and receiver is the most robust.

Except possibly for parallel or quasi-parallel settings, the spatial-wideband effect must be countered for LOS MIMO to behave satisfactorily. Division into subbands is an obvious way, but an exceedingly fine division is required in many cases. A delay-based solution is much more effective and largely satisfactory; moreover, a delay-based solution reinforces the effectiveness of dividing the bandwidth into a small number of subbands.

In terms of how to set the transmit and receive delay lines, minimizing the overall delay spread is an effective strategy, yet there are hints that even better solutions may be possible, and
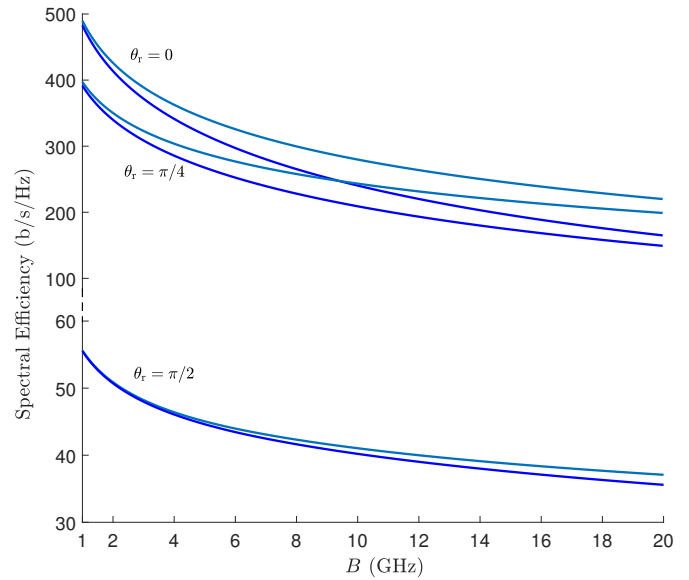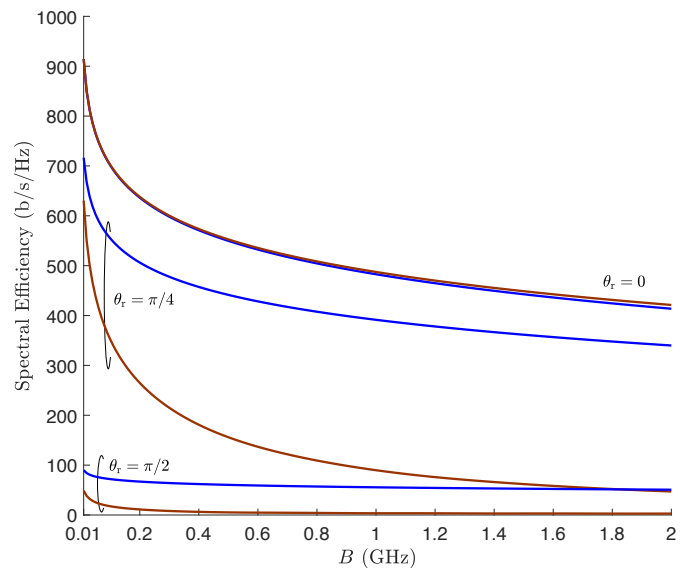


Fig. 10. Spectral efficiency vs bandwidth for $N_{\mathrm{t}} = N_{\mathrm{r}} = 64$, $D = 30$ m, $P/N_0 B = 10$ dB at $B = 20$ GHz, and $f_{\mathrm{c}} = 300$ GHz. Save for $\theta_{\mathrm{r}} = 0$, the bottom curve corresponds to being oblivious to the spatial-wideband effect whereas the top curve corresponds to the use of delay lines.

this presents an avenue of interest for subsequent work. Also of interest is to reassess the performance with estimated time-varying channels, rather than the static channels considered in this paper.

## REFERENCES

[1] I. F. Akyildiz, J. Jornet, and C. Han, "Terahertz band: Next frontier for wireless communications," *Physical Commun.*, vol. 12, pp. 16–32, 2014.

[2] H. Hamada *et al.*, "300-GHz-band 120-Gb/s wireless front-end based on InP-HEMT PAs and mixers," *IEEE Journal of Solid-State Circuits*, vol. 55, no. 9, pp. 2316–2335, 2020.

[3] J.-S. Jiang and M. A. Ingram, "Spherical-wave model for short-range MIMO," *IEEE Trans. Commun.*, vol. 53, no. 9, pp. 1534–1541, 2005.

[4] F. Bohagen, P. Orten, and G. E. Oien, "On spherical vs. plane wave modeling of line-of-sight MIMO channels," *IEEE Trans. Commun.*, vol. 57, no. 3, pp. 841–849, 2009.

[5] M. Matthaiou, A. Sayeed, and J. A. Nossek, "Maximizing LoS MIMO capacity using reconfigurable antenna arrays," in *ITG Workshop on Smart Antennas (WSA)*, 2010, pp. 14–19.

[6] N. Chiurtu and B. Rimoldi, "Varying the antenna locations to optimize the capacity of multi-antenna Gaussian channels," in *Proc. IEEE Int. Conf. Acoust. Speech Signal Process.*, Jun. 2000, pp. 3121–3123.

[7] S. Sun, T. S. Rappaport, R. W. Heath, Jr., A. Nix, and S. Rangan, "MIMO for millimeter-wave wireless communications: Beamforming, spatial multiplexing, or both?" *IEEE Commun. Mag.*, vol. 52, no. 12, pp. 110–121, 2014.

[8] H. Do, N. Lee, and A. Lozano, "Reconfigurable ULAs for line-of-sight MIMO transmission," *IEEE Trans. Wireless Commun.*, vol. 20, no. 5, pp. 2933–2947, 2020.

[9] E. Torkildson, B. Ananthasubramaniam, U. Madhow, and M. Rodwell, "Millimeter-wave MIMO: Wireless links at optical speeds," in *Allerton Conf. Commun., Control and Computing*, 2006, pp. 1–9.

[10] E. Torkildson, U. Madhow, and M. Rodwell, "Indoor millimeter wave MIMO: Feasibility and performance," *IEEE Trans. Wireless Commun.*, vol. 10, no. 12, pp. 4150–4160, Dec. 2011.

[11] X. Song, C. Jans, L. Landau, D. Cvetkovski, and G. Fettweis, "A 60 GHz LOS MIMO backhaul design combining spatial multiplexing and beamforming for a 100 Gbps throughput," in *IEEE Global Commun. Conf.*, Dec. 2015, pp. 1–6.

[12] H. Sarieddeen, M.-S. Alouini, and T. Y. Al-Naffouri, "Terahertz-band ultra-massive spatial modulation MIMO," *IEEE J. Sel. Areas Commun.*, vol. 37, no. 9, pp. 2040–2052, 2019.

[13] C. Lin and G. Y. Li, "Terahertz communications: An array-of-subarrays solution," *IEEE Commun. Mag.*, vol. 54, no. 12, pp. 124–131, Dec. 2016.

[14] H. Do, S. Cho, J. Park, H.-J. Song, N. Lee, and A. Lozano, "Terahertz line-of-sight MIMO communication: Theory and practical challenges," *IEEE Commun. Magazine*, vol. 59, no. 3, pp. 104–109, 2021.

[15] B. Wang, F. Gao, S. Jin, H. Lin, G. Y. Li, S. Sun, and T. S. Rappaport, "Spatial-wideband effect in massive MIMO with application in mmWave systems," *IEEE Communications Magazine*, vol. 56, no. 12, pp. 134–141, 2018.

[16] J. H. Brady and A. M. Sayeed, "Wideband communication with high-dimensional arrays: New results and transceiver architectures," in *2015 IEEE International Conference on Communication Workshop (ICCW)*. IEEE, 2015, pp. 1042–1047.

[17] B. Wang, F. Gao, S. Jin, H. Lin, and G. Y. Li, "Spatial-and frequency-wideband effects in millimeter-wave massive MIMO systems," *IEEE Transactions on Signal Processing*, vol. 66, no. 13, pp. 3393–3406, 2018.

[18] K. Dovelos, M. Matthaiou, H. Q. Ngo, and B. Bellalta, "Channel estimation and hybrid combining for wideband terahertz massive MIMO systems," *IEEE J. Sel. Areas Commun.*, vol. 39, no. 6, pp. 1604–1620, 2021.

[19] H. Hashemi, T.-S. Chu, and J. Roderick, "Integrated true-time-delay-based ultra-wideband array processing," *IEEE Commun. Mag.*, vol. 46, no. 9, pp. 162–172, 2008.

[20] P. Moosbrugger, M. Adkins, and R. Haupt, "Degradation in theoretical phase shift keying waveforms due to signal dispersion in a large communications phased array," in *IEEE Int'l Symp. Phased Array Systems and Techn.*, 2013, pp. 224–226.

[21] T.-S. Chu and H. Hashemi, "True-time-delay-based multi-beam arrays," *IEEE Trans. Microwave Theory and Techniques*, vol. 61, no. 8, pp. 3072–3082, 2013.

[22] A. Tulino, A. Lozano, and S. Verdú, "MIMO capacity with channel state information at the transmitter," in *IEEE Int'l Symp. on Spread Spectrum Techniques and Applications (ISSSTA)*, 2004, pp. 22–26.

[23] Z. Liu, W. ur Rehman, X. Xu, and X. Tao, "Minimize beam squint solutions for 60 GHz millimeter-wave communication system," in *IEEE Veh. Techn. Conf. (VTC Fall)*, 2013, pp. 1–5.

[24] R. W. Heath Jr. and A. Lozano, *Foundations of MIMO Communication*. Cambridge University Press, 2018.